agronomy

MDPI

Article

The Sorption of Sulfamethoxazole by Aliphatic and Aromatic Carbons from Lignocellulose Pyrolysis

Gang Chu [1,*], Zifeng Han [1], Zimo Wang [1], Defeng Kong [1], Wenxiu Qin [1], Youbin Si [1,*], Guozhong Wang [2] and Christian E. W. Steinberg [3]

[1] Anhui Province Key Laboratory of Farmland Ecological Conservation and Pollution Prevention, Faculty of Resources and Environment, Anhui Agricultural University, Hefei 230036, China; 2021116081@stu.njau.edu.cn (Z.H.); htwzm1213@163.com (Z.W.); kdf_001.student@sina.com (D.K.); wxqin@ahau.edu.cn (W.Q.)

[2] Key Laboratory of Materials Physics, Centre for Environmental and Energy Nanomaterials, Institute of Solid State Physics, Chinese Academy of Sciences, Hefei 230031, China; gzhwang@issp.ac.cn

[3] Faculty of Life Sciences, Institute of Biology, Freshwater and Stress Ecology, Humboldt-University at Berlin, Arboretum, Späthstr. 80/81, 12437 Berlin, Germany; christian_ew_steinberg@web.de

* Correspondence: gangchu@aliyun.com (G.C.); youbinsi@ahau.edu.cn (Y.S.)

Abstract: Massive biomass waste with lignocellulose components can be used to produce biochar for environmental remediation. However, the impact of lignocellulose pyrolysis on biochar structure in relation to the sorption mechanism of ionizable antibiotics is still poorly understood. In this paper, diverse techniques including thermogravimetric analysis and ^{13}C nuclear magnetic resonance were applied to investigate the properties of biochars as affected by the pyrolysis of cellulose and lignin in feedstock. Cellulose-derived biochars possessed more abundant groups than lignin-derived biochars, suggesting the greater preservation of group for cellulose during the carbonization. Higher sorption of sulfamethoxazole (SMX) was also observed by cellulose-derived biochars owing to hydrogen bond interaction. Sorption affinity gradually declined with the conversion aliphatic to aromatic carbon, whereas the enhanced specific surface area (SSA) subsequently promoted SMX sorption as evidenced by increased SSA-N_2 and SSA-CO_2 from 350 to 450 °C. The decreased K_d/SSA-N_2 values with increasing pH values implied a distinct reduction in sorption per unit area, which could be attributed to enhanced electrostatic repulsion. This work elucidated the role of carbon phases from thermal conversion of lignocellulose on the sorption performance for sulfonamide antibiotics, which will be helpful to the structural design of carbonaceous adsorbents for the removal of ionizable antibiotics.

Keywords: biochar; lignocellulose pyrolysis; carbon phase; ionizable antibiotics; sorption mechanism

check for updates

Citation: Chu, G.; Han, Z.; Wang, Z.; Kong, D.; Qin, W.; Si, Y.; Wang, G.; Steinberg, C.E.W. The Sorption of Sulfamethoxazole by Aliphatic and Aromatic Carbons from Lignocellulose Pyrolysis. *Agronomy* **2022**, *12*, 476. https://doi.org/10.3390/agronomy12020476

Academic Editor: Baskaran Stephen Inbaraj

Received: 24 December 2021
Accepted: 31 January 2022
Published: 14 February 2022

Publisher's Note: MDPI stays neutral with regard to jurisdictional claims in published maps and institutional affiliations.

Copyright: © 2022 by the authors. Licensee MDPI, Basel, Switzerland. This article is an open access article distributed under the terms and conditions of the Creative Commons Attribution (CC BY) license (https://creativecommons.org/licenses/by/4.0/).

1. Introduction

Biochar is one of the solid carbon-rich products prepared by pyrolysis of biological wastes [1], which has attracted keen interest in its application in environmental remediation including soil fertility and contaminant control [2]. The abundant agricultural and forestry residues, such as bagasse and pine sawdust, provide a substantial potential of biochar production, which is an effective approach to facilitate carbon sequestration and achieve the resource utilization of biomass wastes [3]. Generally, biochar is prepared in a limited-oxygen atmosphere below the pyrolysis temperature of 800 °C [4]. The preparation techniques of biochar involve slow and fast pyrolysis, hydrothermal carbonization, gasification, and microwave irradiation [3,5]. To preserve more chars, slow pyrolysis is widely applied for biochar production on a large scale [6]. Most biological residues experience the conversion of carbon phases under a range of moderate-low temperatures (300–500 °C), which is similar to smoldering wildfires. The pyrolysis techniques and feedstock constituents are regarded as the major factors controlling structure and property of biochars [5]. For example, the conversion of biomass with high lignin content can obtain high-yield

biochars [7]. Ortiz et al. [8] investigated the yield and physico-chemical properties as affected by temperature and composition. They observed that two variables were responsible for all the properties of biochar produced by almond and nut sells, except for yield.

Previous excellent studies have investigated the influence of different feedstocks on biochar preparation [8,9]. For herbs and wooden plants, however, cellulose and lignin are major polymers in the parent feedstock. Cellulose is a linear chain of numerous D-glucose units and the structural component of the primary cell wall of plants [10], whereas lignin is a class of complex organic polymers that form key structural substances in the support tissues of vascular plants [11]. Due to their high shares in biomass, the pyrolysis of both polymers has a crucial influence on the structure and property of biochars. The novelty of this study is to recognize the impact of pyrolysis of lignocellulose in feedstock on the carbonaceous structure and properties, which is essential to the structural design and functional application of biochar in the future.

Sorption by biochar is one of the vital remediation approaches that can alter the migration of environmental contaminants [5]. The application of biochar in soils not only can decrease the utilization of chemical fertilizer [12], but can also control various organic contaminants such as hydrophobic or ionizable compounds [13]. Because of the multilevel structures of biochar, multiple mechanisms are involved in the sorption process. For instance, the hydrophobic effect and π-π interactions have been widely assumed to be the crucial driving force for the sorption of hydrophobic compounds [14]. Wang et al. [15] investigated that the sorption behavior of hydrophobic compounds by biochars and found that the hydrophobic effect was responsible for the organic sorption through the aromatic moieties. Peng et al. [16] reported that the strong correlation between the number of π-rings and sorption of antibiotics implied that π-π interaction was the dominating sorption mechanism. For ionic organics, their speciation relies on the pH and thereby affects their sorption affinity. Once the compounds are dissociated, the electrostatic interaction will occur inevitably: (a) electrostatic attraction will occur if the biochar and compound possess unlike charges; (b) electrostatic repulsion will occur if the biochar and compound exhibit identical charges. Zhao et al. [17] explored the sorption performance of biochar coated with humic acid for fluoroquinolone antibiotics and pointed out that the electrostatic attraction contributed to the apparent sorption.

As veterinary drugs and feed additives, sulfonamide antibiotics are applied to the treatment of bacterial diseases during industrial livestock and poultry breeding [18]. The excrements have widely been used to fertilize farmland soils after storage and disposal. However, through this method, a plethora of trace antibiotics is discharged into cultivated land, surface water, as well as groundwater. For instance, the concentration of sulfonamides was evaluated to be up to 14.56 μg/L in swine wastewater as reported by Ben et al. [19]; 4.5 μg/kg sulfamethazine were found in a top 0–30-cm soil [20]. The wide application of sulfonamide antibiotics causes adverse effects on ecological safety and human health, thereby drawing increasing attention to public health concerns. Zhao et al. [21] focused on the contribution of biochar minerals to the sorption of ionizable sulfamethoxazole and found that the demineralization could increase the sorption. The removal of sulfonamide antibiotics was investigated by activated carbon and graphene-based materials as reported by Luo et al. [22]. They observed that the granular wood-derived activated carbon exhibited the largest sorption (~258.7 mg/g) for sulfamethoxazole among the carbonaceous materials. If the structural property of biochar as affected by lignocellulose pyrolysis is unclear, an inaccurate or risky prediction may occur for sorption behavior once biochar application is running. Therefore, it is crucial to identify how the pyrolysis of cellulose and lignin influence the biochar properties and is necessary to achieve robust understanding of the underlying sorption mechanisms for sulfonamide antibiotics.

In this work, the sulfamethoxazole (SMX), belonging to one representative sulfonamide antibiotic and ionizable organic contaminant, was selected as a target adsorbate to explore its sorption behavior. Biochars were produced by anaerobic pyrolysis of bagasse, pine sawdust, cellulose, and lignin. Combined with multiple techniques, the structural

properties of biochars with respect to SMX sorption mechanisms were discussed. This work will provide fundamental support for smart design of biochar structure and establish a structure-function relationship to accurate prediction the sorption behavior of ionic antibiotics after biochar application.

2. Material and Methods

2.1. Materials and Chemicals

Bagasse (BA) and pine sawdust (PS) were collected from the agricultural-trade and wood-processing market, respectively. The compositions of cellulose, hemicellulose, and lignin of BA and PS can be referred to in Table S1 [23,24]. After oven drying at 65 °C, both biomass wastes were ground to obtain particles with less than 100 meshes for biochar production. Cellulose (CE), and lignin (LI) (Sigma-Aldrich), as the model feedstocks, were also used to produce biochars. SMX, hydrochloric acid (HCl), sodium chloride (NaCl), sodium azide (NaN_3), and sodium hydroxide (NaOH) (analytical grade reagents) were purchased from Aladdin Bio-Chem Technology Co. (Beijing, China). Selected properties of SMX are listed in Table S2.

2.2. Biochar Preparation

BA, PS, CE, and LI were placed in ceramic crucibles into a muffle furnace and pyrolyzed under N_2 atmosphere for 4 h at 250, 350, and 450 °C, respectively. The selected temperature range was dependent on main decomposition of lignocellulose in feedstock. Solid carbonaceous particles were respectively prefixed as BA-X, PS-X, CE-X, and LI-X, where X referred to the pyrolytic temperatures. Subsequently, all samples were repeatedly washed with deionized water to pH 6.5 (solid to liquid ratio of 1:20). Then they were dried and stored for the characterization and sorption experiments.

2.3. Characterization of Biochars

The pyrolysis behavior of biomass feedstocks was analyzed by the thermogravimetric analyzer with differential scanning calorimetry (TG-DSC) (STA 449F3, Netzsch, Germany) under a nitrogen atmosphere. The total elemental composition was measured by an Elementar analyzer (Vario MicroCube, Elementar, Germany). The physical adsorption instruments (Autosorb-1C, Quantachrome, Boynton Beach, FL, USA) with N_2 and CO_2 models were applied to measure the specific surface area (SSA) from mesopores (2–50 nm) and micropores (0.4–1.5 nm), respectively. Owing to the limitation of N_2 diffusion into micropores at −196 °C, we estimated the micropore structure by CO_2 adsorption at 0 °C. The SSA-N_2 and SSA-CO_2 were calculated by the BET and DFT methods, respectively. The carbon phases (aliphatics and aromatics) of bicohars were probed with the solid-state ^{13}C nuclear magnetic resonance (NMR) spectrometer (JNM-ECZ600R, JEOL, Tokyo, Japan). The surface charges of biochars were determined by a Zeta potential analyzer (90Plus, NanoBrook, Holtsville, NY, USA). The Fourier transform infrared spectrometer (FTIR) (Varian 640-IR, Agilent, Santa Clara, CA, USA) was applied to explore the polar functional groups of all biochars in the range of 400–4000 cm^{-1}. The acid-base titrations were carried out to determine the content of carboxyl and phenol groups. Briefly, 100 mg of biochar particles were mixed with 100 mL of background solution that was adjusted by 0.1 mol/L HCl solution to pH 2 in beaker. Subsequently, a certain amount (0.01–0.02 mL) of 0.01 mol/L NaOH solution was unceasingly added by a pipette. After sufficiently stirring the solution, the stable pH value was documented by a pH meter from pH 3 to pH 11. Then the acid-base titration curves were obtained based on the above-mentioned method.

2.4. Sorption Experiment

The background solution contained 0.02 mol/L NaCl (as electrolyte) and 200 mg/L of NaN_3 (as biocide) to prepare SMX solution with 9 concentrations. Batch sorption experiment in the concentration range of 1–50 mg/L was performed in 8 mL glass vials sealed with Teflon-lined septum screw cap. Based on the preliminary studies [21], the

ratio of solid to liquid fractions was determined as 1:1000 (m/v). The pH value of SMX solution was adjusted to 4.0 and 7.0 with 0.1 and 0.01 mol/L HCl or NaOH. All glass vials were shaken in the dark in a shaker at 25 °C for 7 d to reach equilibrium. Two replications were carried out. After 3000 rpm centrifugation, the supernatant of vials was sampled to quantify the aqueous concentrations with the high-performance liquid chromatography (HPLC) (Agilent 1200, Agilent Technologies, Santa Clara, CA, USA).

2.5. Data Analysis

Freundlich and Dubinin-Ashtakhov models were applied to fit the sorption isotherms with SigmaPlot 10.0.

$$\text{Freundlich model (FM): } S_e = K_F\, C_e{}^n \quad (1)$$

$$\text{Dubinin-Ashtakhov model (DAM): } \ln S_e = \ln Q^0 - (\varepsilon/E)^{\,b} \quad (2)$$

where K_F [(mg/g)/(mg/L) ^{n}] is the sorption coefficient and n refers to the nonlinearity factor. The S_e (mg/g) and C_e (mg/L) are, respectively, the solid- and aqueous-phase concentrations when sorption reached the equilibrium. Q^0 (mg/kg) refers to the sorption capacity at saturation. $\varepsilon = R\ T\ \ln(C_s/C_e)$ (J/mol) is the effective sorption potential. R [8.314 J/(mol·K)] is the universal gas constant; T (K) is the absolute temperature; C_s (mg/L) is the water solubility of the sorbate. E (J/mol) is the correlating divisor; and b is the fitting parameter.

3. Results and Discussion

3.1. Pyrolysis Characteristics

TG-DSC curves of the feedstocks are illustrated in Figure 1. The pyrolysis process can be divided into three stages: dehydration, cyclization, and condensation [23]. CE decomposition was less than 6.2% before reaching 270 °C through the intermolecular or intramolecular dehydration. Subsequently, more than 82.2% of CE was decomposed in the range of 270–390 °C. During the cyclization process, an exothermic phenomenon was distinctly observed as illustrated by the DSC curves [24]. At the condensation stage, the volatile matter was less than 3.2% and a series of aromatic units evolved into condensed conjugated sheets. By comparison with CE pyrolysis, LI underwent the decomposition in larger temperature range from 200 to 600 °C and more carbonaceous residues (around 46%) were preserved during LI pyrolysis. This result is attributed to the thermal endurance of the majority of aromatic rings in LI [23]. The initial LI contains numerous cross-linking phenolic structures that contribute significantly to the formation of aromatic carbon in biochar.

Yields of BA- and PS-derived biochars showed a substantial decline with increasing temperatures. The mass loss of BA and PS began at 200 °C and primarily occurred from 200 to 400 °C. When temperature reached 450 °C, the yields were 17.8% and 17.6% for BA450 and PS450, respectively. Subsequently, TG curves tended to flatten out above 500 °C. It was found that the pyrolysis behavior of BA and PS encompassed superimposed decomposition process of CE and LI. For instance, there were two peaks occurring at 298 and 360 °C, respectively. The first one belonged to LI decomposition at the rate of 0.5 %/°C, while the second one referred to CE decomposition with the exothermic phenomenon of 10 mW/mg. Compared to BA degradation, more LI was decomposed during the pyrolysis process of PS. Shi et al. [25] reported that the LI content accounted for 25.3% in PS, while the LI content of BA was around 21.6% as quantified by Moraes Rocha et al. [26].

3.2. Evolution of Carbon Structure

As the pyrolytic temperature increased, the C content increased and O content decreased (Table 1). The declined H/C and O/C values implied an enhancement of aromaticity and a reduction in polarity of the biochars. The ^{13}C NMR spectra provide information on carbon components of the biochars (Figure 2a). The alkyl-C and alkyl-O components were greatly similar to those of humic substance in soils and sediments [27]. These alkyl moieties subsequently evolved to aryl moieties along with the rapid escape of volatile

organic matter during the intensified carbonization. Thus, the aliphaticity decreased but the aromaticity increased for biochars with increasing pyrolysis temperatures (Table 1). It was worth noting that CE-derived biochars exhibited stronger the aliphaticity than LI-derived biochars. Likewise, the aliphaticity of BA-derived biochars was slightly higher than those of PS-derived biochars probably due to more CE content in BA.

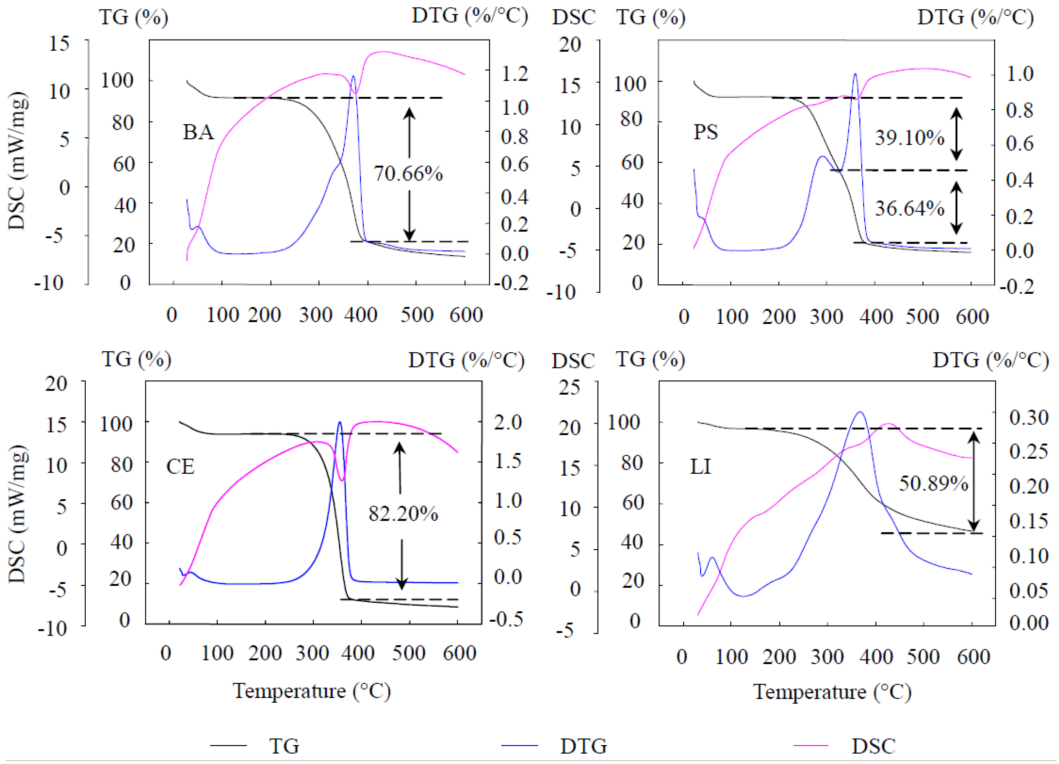

Figure 1. The thermogravimetric analysis with differential scanning calorimetry (TG-DSC) of BA, PS, CE, and LI in the temperature range of 100–600 °C. The exo represent the exothermic direction of DSC curves.

Table 1. The elemental composition, carbon phases, and SSA of various biochars.

Samples	Bulk Elemental Composition (%)					Ali [a]	Aro [a]	SSA (m^2/g) [b]	
	C	O	H	H/C	O/C	(%)	(%)	N_2	CO_2
BA250	53.50	39.84	5.60	1.26	0.56	68.84	31.16	20.27	106.94
BA350	67.49	24.58	3.91	0.70	0.27	51.65	48.35	19.86	291.50
BA450	71.45	21.01	3.53	0.59	0.22	45.93	54.07	91.95	370.24
PS250	58.37	33.62	5.33	1.10	0.43	66.44	33.56	15.37	116.96
PS350	71.89	22.63	4.08	0.68	0.24	49.05	50.95	15.13	269.35
PS450	76.24	20.54	3.70	0.58	0.20	45.25	54.75	70.52	341.24
CE250	48.72	48.87	6.52	1.61	0.75	79.16	20.84	15.87	47.39
CE350	70.23	28.22	3.91	0.67	0.30	53.06	46.94	17.31	339.65
CE450	78.09	18.63	3.46	0.53	0.18	42.78	57.22	40.19	436.11
LI250	66.41	25.48	5.53	1.00	0.29	55.16	44.84	17.64	58.43
LI350	69.93	23.81	3.95	0.68	0.26	46.72	53.28	16.07	276.68
LI450	74.99	19.56	3.47	0.55	0.20	41.83	58.19	53.17	385.72

[a] Ali and Aro (%) refer to the aliphaticity and aromaticity of biochar based on ^{13}C NMR calculation; [b] SSA (m^2/g) refers to the specific surface area from mesopores (by N_2 adsorption) and micropores (by CO_2 adsorption), respectively.

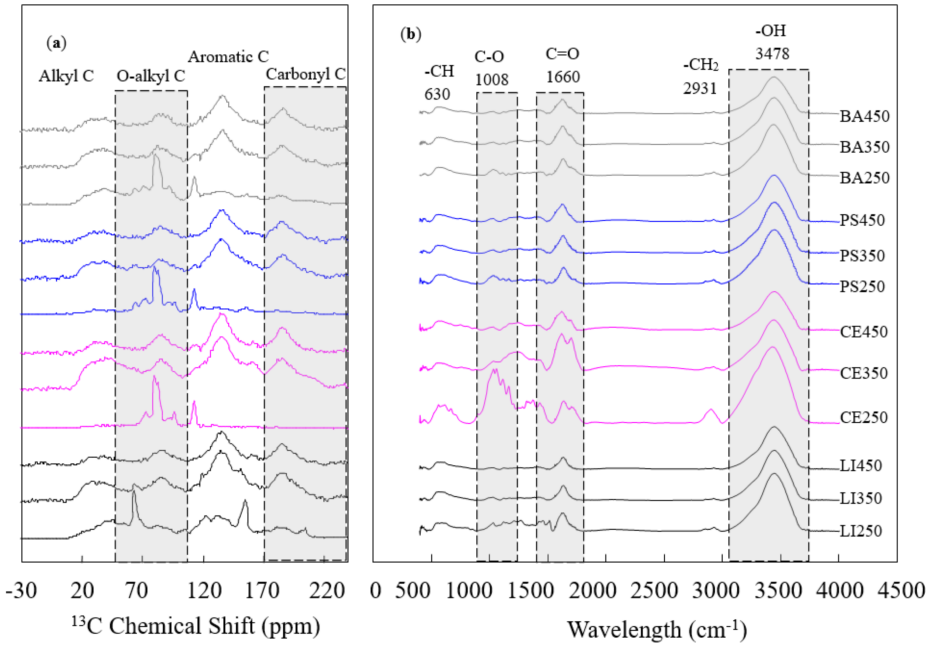

Figure 2. ^{13}C NMR (**a**) and FTIR (**b**) spectra of biochars from lignocellulose pyrolysis at different temperatures. The grey, blue, pink, and black line represented the BA-, PS-, CE-, and LI-derived biochars, respectively.

The conversion into aromatic carbon facilitated the generation of porous structure. For instance, the SSA-CO_2 of BA-derived biochars increased from 106.94 to 370.24 m^2/g with increasing aromaticity. A significantly positive correlation between aromaticity and SSA-CO_2 suggests the wide generation of micropores with the evolution of aromatic carbon (Figure S1). Moreover, the potential of CE exhibits the superiority over that of LI in micropore generation, probably due to the crystal lattice structure of CE during carbonization (Table 1). It was worth noting that the development of mesopores distinctly lags behind the micropore generation in the temperature range of 250–450 °C. The pressures on the wall of substantial micropores were increased by the rising of pyrolytic temperatures so that may result in the collapse of partial micropores to mesopore formation. The mesopores of BA450 and PS450 abruptly soared, as illustrated by SSA-N_2 values. It was seen that the explosive development of mesopores was strongly dependent on the transformation of condensed carbon phase. Scanning electron microscope (SEM) images provided the surface morphology of biochars and also evidenced the development of mesopore structures (Figure S2).

The pore system would concentrate and sequester contaminants in the aqueous phase. Previous studies have revealed that pore-filling is one important mechanism for organic sorption by biochars as shown with polycyclic aromatic hydrocarbons [28,29], nonylphenol [30], or pharmaceuticals, and bisphenol A [31]. Studying hydrophobic contaminants, these authors confirmed that the volume and size of nanopores were the critical factors to pore-filling mechanism. Nevertheless, the question arises whether this mechanism is generalizable with sorption also for ionizable sulfonamide antibiotics. Thus, further work is required to explore the interfacial sorption behavior between ionizable compounds and biochars.

3.3. Surface Functional Groups

In the FTIR spectra (Figure 2b), the broadband at 3478 cm^{-1} represented the stretching vibration of −OH in crystal and adsorbed water. The peak at 2931 cm^{-1} corresponded to the vibration of $-CH_2$ of alkyl structure for aliphatic carbons. At 1660 cm^{-1} and 1008 cm^{-1}, the characteristic peaks referred to the intensity of alcohol C-O and carboxyl C=O, respectively [2]. Three phenomena were observed by the FTIR spectra. First, the

vibration intensity of chemical bonds gradually decreased with increasing temperature, demonstrating the elimination of functional groups. Second, no detectable distinction in FTIR spectra was observed for BA and PS-derived biochars, indicating that both BA and PS experience similar chemical transformation processes. Finally, in comparison with the spectra of LI-derived biochars, CE-derived biochars possessed abundant C-O and C=O groups (at 1008 and 1660 cm^{-1}) in the alcohols, aldehydes, or ketones.

In general, it is agreed that the acidity of biochars is dependent on the adjustment by carboxyl and phenol groups [32]. To be specific, the content of carboxyl groups equaled the alkali consumption in the pH range of 3–8; the content of phenol groups was estimated as twice the alkali consumption from pH 8 to pH 10 (Figure 3). Consistent with the FTIR spectra, acidic groups of CE-derived biochars were more abundant than those of LI-derived biochars as shown by titration curves. BA-derived biochars also exhibited more acidic groups compared with PS-derived biochars, especially for phenol groups (Table S3). The results indicate that the feedstocks with high CE appear to be conducive to the preservation of functional groups of biochars during the pyrolysis. These polar functional groups are in close relation to the surface charges of biochars. The surface charges as affected by pHs are presented in Figure 3. All biochars had negative charges and these negative charges gradually increased with the rising pH. For example, the negative charges of BA350 increased from −16.8 mV to −47.33 mV in the pH range of 3 to 11. The phenomenon could be resulted from the dissociation of groups in aqueous phase. As a result, BA- and CE-derived biochars possessed more negative charges than PS- and LI-derived biochars, respectively.

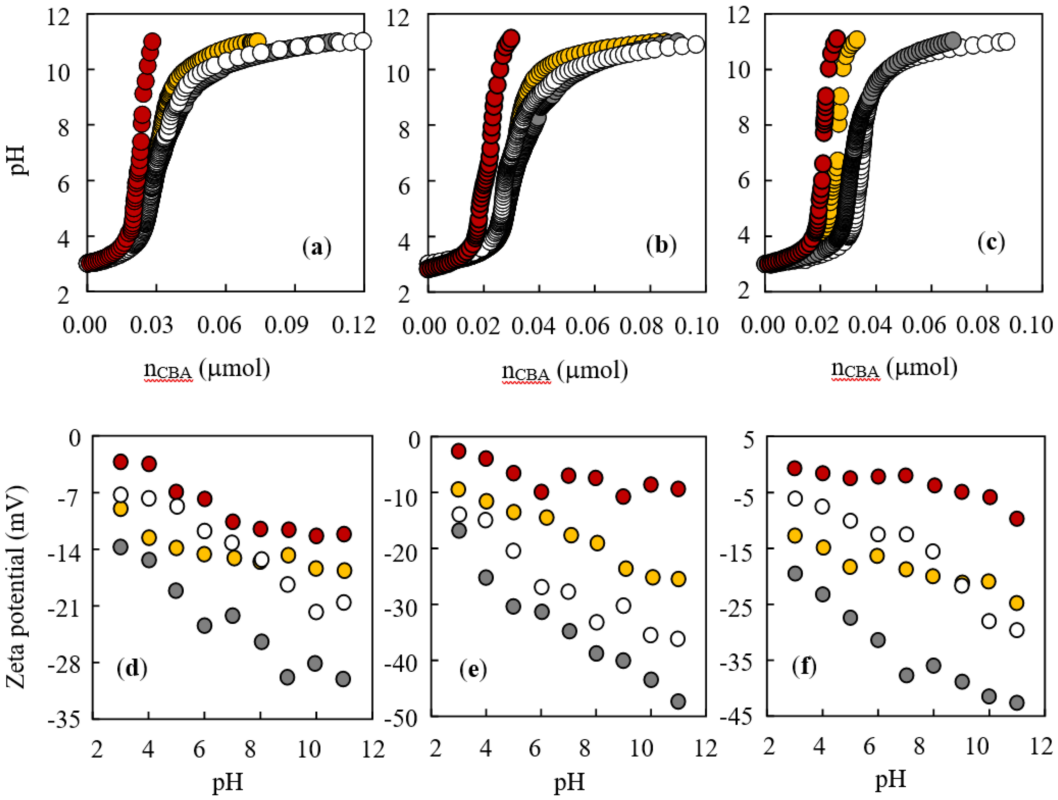

Figure 3. Titration of acidic groups (**a**,**b**,**c**) and Zeta potential (**d**,**e**,**f**) of biochars at 250, 350 and 450 °C, respectively. The grey, yellow, white, and red symbols referred to BA-, PS-, CE-, and LI-derived biochars, respectively.

3.4. Isothermal Sorption

Sorption isotherms of SMX are presented for various biochars at pH 4 and 7 (Figure 4). First, both the aliphatic and aromatic carbon phases contributed to apparent capacity of SMX sorption through hydrophobic interaction. For biochar at 250 °C, the carbon structure

just suffered from the dehydration and cyclization reaction and their aliphaticity of biochars was higher than 65%, except for LI-derived biochar. The aliphatic carbon such as alkyl component may be mainly responsible for sorption capacity. However, it was seen that the apparent sorption began to decrease with the evolution of aliphatic into aromatic carbons at 350 °C. Although the micropores had been developed in the aromatic domain, the steric hindrance of microporous sorbents may exist for the large-molecule sorbates in the sorption system [33]. Subsequently, when the pyrolysis temperature reached 450 °C, most of the volatile matter, such as phenol groups, had been released and the micropore wall could be frangible, leading to the generation of mesopore structures that gradually came into effect in the sorption process. It was observed that SMX sorption was enhanced again for BA450 and PS450. Ji et al. [34] pointed out the size exclusion affected the sorption of SMX and tetracycline by biochars. The increased mesoporosity and reduced diffusion restriction greatly improved the sorption of ionizable compounds as reported by Xiao and Pignatello [35]. Feng et al. [36] emphasized the importance of mesopores in biochar derived from corn straw to the sorption of phenol. Compared with DAM, FM showed broader applicability for fitting isotherms as illustrated by high R_{adj}^2 (Table S4). The nonlinearity of sorption was expressed by the nonlinear factor (n) ranging from 0.46 to 0.89, indicating the heterogeneity of the apparent sorption by biochars. The heterogeneous sorption was observed because of the distribution of porous structure in condensed aromatic carbons. This nonlinear sorption for SMX was influenced by the porous structure as reported by Zheng et al. [37].

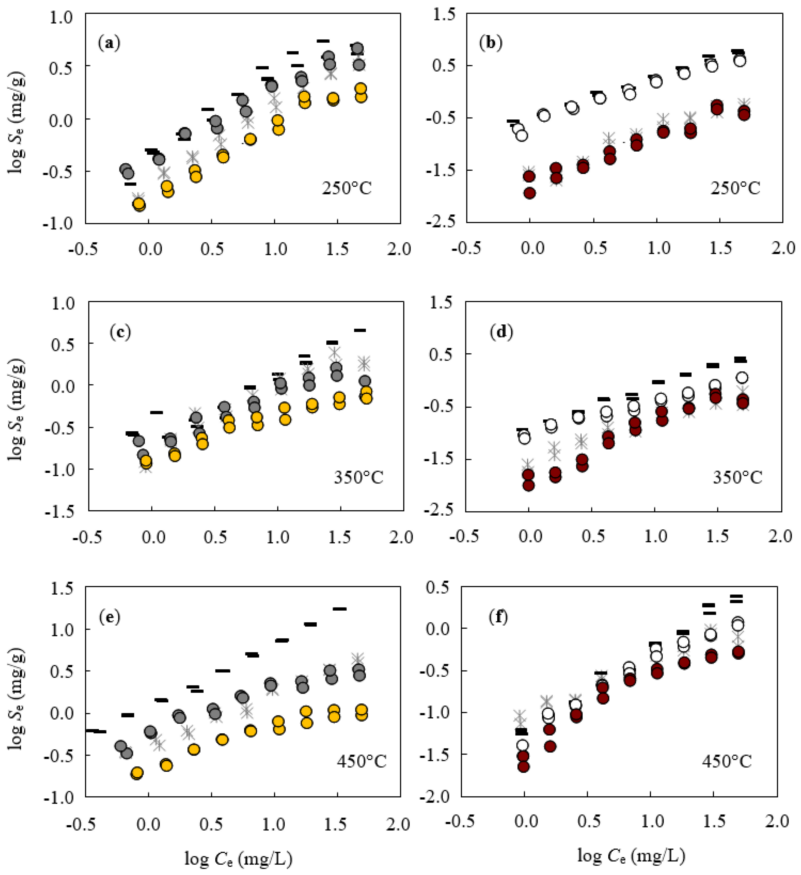

Figure 4. Sorption isotherms on various biochars at pH 4 (thin fork, horizontal mark) and pH 7 (circular rings). The grey and yellow circular rings represented BA- and PS-derived biochars produced at 250 (**a**), 350 (**c**) and 450 °C (**e**); the white and red circular rings represented CE- and LI-derived biochars produced at 250 (**b**), 350 (**d**) and 450 °C (**f**), respectively.

Second, BA-and CE-derived biochars respectively exhibited larger sorption than PS- and LI-derived biochars at the same temperature. The results indicated that carbon component produced from CE was conducive to form a close affinity with SMX. According to the titration calculation (Table S3), it was found that CE-derived biochars possessed more abundant phenol groups (0.018–0.032 μmol/g) than LI-derived biochars (0.003–0.006 μmol/g). These phenol groups in aliphatic component endowed carbon structure with better compatibility with SMX molecules. This may be attributed to hydrogen bond interaction that extensively occurs between phenol groups (−OH) of biochar and amine groups of SMX^0 ($-NH_2$) [38]. The hydrogen bond interaction facilitates the hydrophobic partition process for majority of SMX. However, with the elimination of polar functional groups, especially for −OH groups, a distinct reduction in SMX sorption was observed for CE-derived biochars due to the declined hydrogen bond interaction. Moreover, as the pyrolytic temperature was raised, the difference in sorption capacity was unceasingly decreased between CE- and LI-derived biochars.

3.5. Sorption as Affected by pH Values

Normalization of sorption coefficients (K_d) by SSA of adsorbates is a widely applied approach to exclude the role of pore structure on apparent sorption. The normalization of K_d by SSA-N_2 were calculated at the initial concentration of 7.0 mg/L. The K_d/SSA-N_2 as affected by pH is presented in Figure 5. The following discussion will be on the basis of calculated K_d/SSA-N_2 values. One observation was that the K_d/SSA-N_2 successively diminished for CE-derived biochars, whereas no obvious distinction was observed for LI-derived biochars with the rising of pyrolytic temperature. The result indicates that porous structure could not be main domains controlling the sorption of ionizable SMX by CE-derived biochars. The decrease in sorption affinity of CE-derived biochars per unit area was attributed to the declined hydrogen bond interaction owing to the massive destruction of phenol groups.

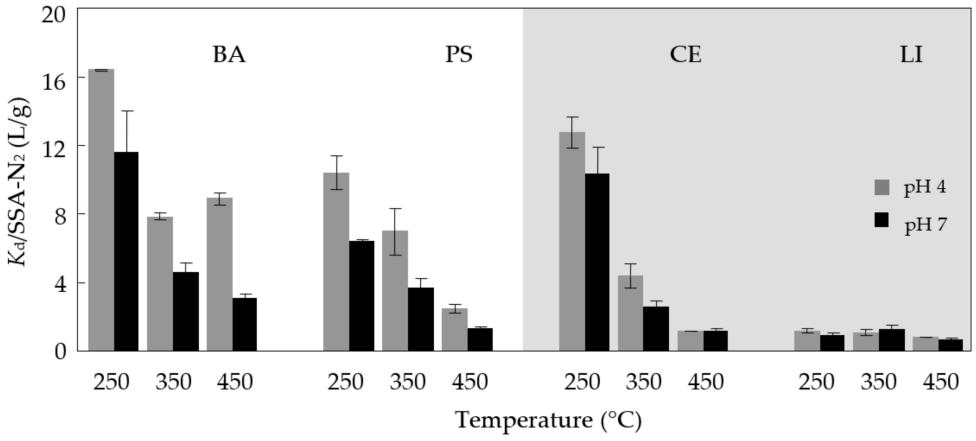

Figure 5. Normalization of sorption coefficients (K_d) by SSA-N_2 on the calculation of initial concentration of 7.0 mg/L onto biochars at pH4 and pH7.

On the other hand, the neutral molecules could dissociate into anionic species as the pH of solution is increased. The SMX^0 prevails (around 96%) at pH 4, whereas the proportion of anionic SMX^- accounted for 97.2% at pH 7 based on the species calculation (Table S2). Because of the ionization, the polar functional groups including phenol and carboxyl groups, contributed significantly to the negative charges of biochars. The other observation was that K_d/SSA-N_2 significantly decreased by 20–45% with the rising pH values (except for LI-derived biochars). In particular, the shrinking K_d/SSA-N_2 of biochars from CE component implied the substantial reduction in sorption capacity per unit area. The results were ascribed to the enhanced electrostatic repulsion between ionic SMX^- and

negatively charged particles. Wu et al. [39] evidenced that the electrostatic repulsion played a vital role in SMX sorption on the biochar derived from sediments.

On the basis of the discussion above, a concept map of carbon phases with regard to sorption mechanisms is illustrated in Figure 6. Biochar consists of diverse carbon phases from lignocellulose decomposition with pyrolysis temperature. The hydrophobic effect forced SMX^0 to encounter the carbonaceous surface in the aqueous phase. The hydrogen bond interaction between phenol and amine groups also greatly promoted sorption affinity to SMX^0 on aliphatic carbons. As the aliphatic carbon evolved into aromatic ones with increasing temperature, the sorption capacity gradually decreased due to the declined hydrogen bond interaction. On the other hand, the generated nanopores in aromatic carbon started to facilitate the apparent sorption. Nevertheless, when the anionic species increased with the rising of pH, the electrostatic repulsion was strongly enhanced between anionic SMX^- and negative charged biochars, resulting in the restriction of SMX sorption. Overall, multiple mechanisms are involved in the sorption process for sulfonamide contaminants including the hydrophobic partition, the hydrogen bonding effect, pore-filling, and electrostatic interaction.

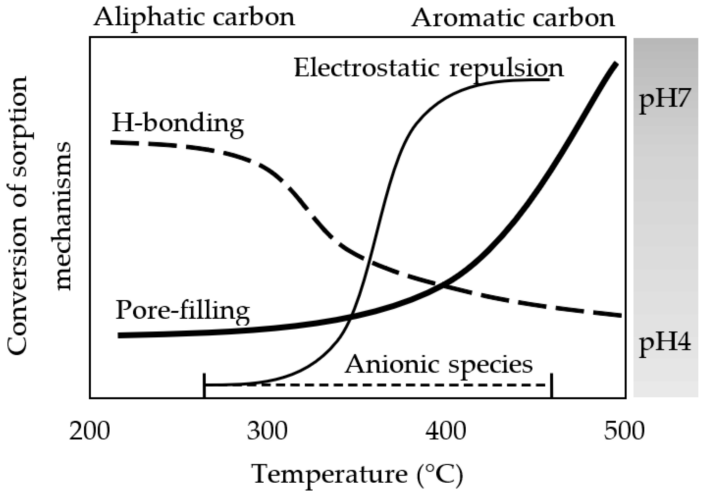

Figure 6. The concept of possible mechanisms for SMX sorption by carbon phases (aliphatic and aromatic carbons) from lignocellulose pyrolysis.

4. Conclusions

This research focused on the evolution of carbon phases through the pyrolysis of lignocellulose components. The thermal conversion of BA and PS included the decomposition of CE and LI. Although less mass loss was observed during LI pyrolysis, CE-derived biochar exhibited more excellent potential in group preservation and pore generation. These structural properties made CE-derived biochars to be more conducive to SMX sorption through hydrogen bonding and pore-filling effect. The hydrogen bonding effect declined and pore-filling came into effect as the aliphatic carbons evolved to aromatic ones. Besides, the enhanced electrostatic repulsion between SMX- could inhibit the sorption capacity with the rising of pH values. This work clearly provides evidences for adsorptive mechanisms of SMX by aliphatic and aromatic carbons, which will make for the evaluation of environmental behavior of sulfonamide antibiotics after biochar application.

Supplementary Materials: The following supporting information can be downloaded at: https://www.mdpi.com/article/10.3390/agronomy12020476/s1, Figure S1: The correlation between O/C and aliphaticity (a), H/C and aromaticity (b), SSA-CO_2 and aromaticity (c) for biochars from BA, PS, CE, and LI. Figure S2: Scanning electron microscope (SEM) images of biochars from BA, PS, CE, and LI, respectively. Table S1. The content of CE, hemicellulose and LI in biomasses according to the literatures. Table S2. Selected physico-chemical properties of sulfamethoxazole. Table S3.

The titration results of acidic groups of biochars. Table S4. Fitting results of sorption isotherms of sulfamethoxazole on biochars.

Author Contributions: Conceptualization, G.C.; data curation, Z.H. and Z.W.; formal analysis, D.K.; funding acquisition, G.C.; investigation, Z.H.; methodology, Z.W.; project administration, G.C.; resources, Y.S., G.W. and W.Q.; supervision, Y.S.; validation, D.K.; visualization, G.C.; writing—original draft, G.C.; writing—review and editing, G.C., Y.S. and C.E.W.S. All authors have read and agreed to the published version of the manuscript.

Funding: This work was supported by the National Natural Science Foundation of China (42107406), the University Natural Science Research Project of Anhui Province (KJ2019A0204), and the Natural Science Foundation of Anhui Province (2008085QD186).

Institutional Review Board Statement: Not applicable.

Informed Consent Statement: Not applicable.

Data Availability Statement: The data presented in this work are available on request from the corresponding author.

Acknowledgments: We thank Yang Liu from Faculty of Environment Science and Engineering, Kunming University of Science and Technology (China) for reviewing a draft of this manuscript.

Conflicts of Interest: The authors declare no conflict of interest.

References

1. Wang, D.; Jiang, P.; Zhang, H.; Yuan, W. Biochar production and applications in agro and forestry systems: A review. *Sci. Total Environ.* **2020**, *723*, 137775. [CrossRef] [PubMed]
2. Chu, G.; Zhao, J.; Liu, Y.; Lang, D.; Wu, M.; Pan, B.; Steinbergd, C.E.W. The relative importance of different carbon structures in biochars to carbamazepine and bisphenol a sorption. *J. Hazard. Mater.* **2019**, *373*, 106–114. [CrossRef] [PubMed]
3. Xiao, X.; Chen, B.; Chen, Z.; Zhu, L.; Schnoor, J.L. Insight into multiple and multilevel structures of biochars and their potential environmental applications: A Critical Review. *Environ. Sci. Technol.* **2018**, *52*, 5027–5047. [CrossRef] [PubMed]
4. Pignatello, J.J.; Mitch, W.A.; Xu, W. Activity and reactivity of pyrogenic carbonaceous matter toward organic compounds. *Environ. Sci. Technol.* **2017**, *51*, 8893–8908. [CrossRef]
5. Lian, F.; Xing, B. Black carbon (biochar) in water/soil environments: Molecular structure, sorption, stability, and potential risk. *Environ. Sci. Technol.* **2017**, *51*, 13517–13532. [CrossRef]
6. Torres-Sciancalepore, R.; Fernandez, A.; Asensio, D.; Riveros, M.; Fabani, M.P.; Fouga, G.; Rodriguez, R.; Mazza, G. Kinetic and thermodynamic comparative study of quince bio-waste slow pyrolysis before and after sustainable recovery of pectin compounds. *Energy Convers. Manag.* **2022**, *252*, 115076. [CrossRef]
7. Liu, W.J.; Jiang, H.; Yu, H.Q. Development of biochar-based functional materials: Toward a sustainable platform carbon material. *Chem. Rev.* **2015**, *115*, 12251–12285. [CrossRef]
8. Ortiz, L.R.; Torres, E.; Zalazar, D.; Zhang, H.; Rodriguez, R.; Mazza, G. Influence of pyrolysis temperature and bio-waste composition on biochar characteristics. *Renew. Energy* **2020**, *155*, 837–847. [CrossRef]
9. Al-Rumaihi, A.; Parthasarathy, P.; Fernandez, A.; Al-Ansari, T.; Mackey, H.R.; Rodriguez, R.; Mazza, G.; McKay, G. Thermal degradation characteristics and kinetic study of camel manure pyrolysis. *J. Environ. Chem. Eng.* **2021**, *9*, 106071. [CrossRef]
10. Klemm, D.; Heublein, B.; Fink, H.P.; Bohn, A. Cellulose: Fascinating biopolymer and sustainable raw material. *Angew. Chem. Int. Ed.* **2005**, *44*, 3358–3393. [CrossRef]
11. Sjöström, E. *Lignin in Wood Chemistry*; Academic Press: San Diego, CA, USA, 1993; pp. 71–89.
12. Harvey, O.R.; Kuo, L.-J.; Zimmerman, A.R.; Louchouarn, P.; Amonette, J.E.; Herbert, B.E. An index-based approach to assessing recalcitrance and soil carbon sequestration potential of engineered black carbons (biochars). *Environ. Sci. Technol.* **2012**, *46*, 1415–1421. [CrossRef] [PubMed]
13. Jin, J.; Kang, M.; Sun, K.; Pan, Z.; Wu, F.; Xing, B. Properties of biochar-amended soils and their sorption of imidacloprid, isoproturon, and atrazine. *Sci. Total. Environ.* **2016**, *550*, 504–513. [CrossRef] [PubMed]
14. Keiluweit, M.; Kleber, M. Molecular-level interactions in soils and sediments: The role of aromatic pi-systems. *Environ. Sci. Technol.* **2009**, *43*, 3421–3429. [CrossRef] [PubMed]
15. Wang, Z.; Han, L.; Sun, K.; Jin, J.; Ro, K.S.; Libra, J.A.; Liu, X.; Xing, B. Sorption of four hydrophobic organic contaminants by biochars derived from maize straw, wood dust and swine manure at different pyrolytic temperatures. *Chemosphere* **2016**, *144*, 285–291. [CrossRef] [PubMed]
16. Peng, B.; Chen, L.; Que, C.; Yang, K.; Deng, F.; Deng, X.; Shi, G.; Xu, G.; Wu, M. Adsorption of antibiotics on graphene and biochar in aqueous solutions induced by pi-pi interactions. *Sci. Rep.* **2016**, *6*, 31920. [CrossRef] [PubMed]
17. Zhao, J.; Liang, G.; Zhang, X.; Cai, X.; Li, R.; Xie, X.; Wang, Z. Coating magnetic biochar with humic acid for high efficient removal of fluoroquinolone antibiotics in water. *Sci. Total. Environ.* **2019**, *688*, 1205–1215. [CrossRef] [PubMed]

18. Zhou, X.; Wang, J.; Lu, C.; Liao, Q.H.; Gudda, F.O.; Ling, W.T. Antibiotics in animal manure and manure-based fertilizers: Occurrence and ecological risk assessment. *Chemosphere* **2020**, *255*, 127006. [CrossRef]
19. Ben, W.W.; Pan, X.; Qiang, Z.M. Occurrence and partition of antibiotics in the liquid and solid phases of swine wastewater from concentrated animal feeding operations in Shandong Province, China. *Environ. Sci. Process. Impacts* **2013**, *15*, 870–875. [CrossRef]
20. Sarmah, A.K.; Meyer, M.T.; Boxall, A.B.A. A global perspective on the use, sales, exposure pathways, occurrence, fate and effects of veterinary antibiotics (VAs) in the environment. *Chemosphere* **2006**, *65*, 725–759. [CrossRef]
21. Zhao, J.; Zhou, D.; Zhang, J.; Li, F.; Chu, G.; Wu, M.; Pan, B.; Steinberg, C.E.W. The contrasting role of minerals in biochars in bisphenol A and sulfamethoxazole sorption. *Chemosphere* **2021**, *264*, 128490. [CrossRef]
22. Luo, B.; Huang, G.; Yao, Y.; An, C.; Zhang, P.; Zhao, K. Investigation into the influencing factors and adsorption characteristics in the removal of sulfonamide antibiotics by carbonaceous materials. *J. Clean. Prod.* **2021**, *319*, 128692. [CrossRef]
23. Shi, X.; Wang, J. A comparative investigation into the formation behaviors of char, liquids and gases during pyrolysis of pinewood and lignocellulosic components. *Bioresour. Technol.* **2014**, *170*, 262–269. [CrossRef]
24. Rocha, G.J.d.; Nascimento, V.M.; Goncalves, A.R.; Silva, V.F.N.; Martin, C. Influence of mixed sugarcane bagasse samples evaluated by elemental and physical-chemical composition. *Ind. Crop. Prod.* **2015**, *64*, 52–58. [CrossRef]
25. Collard, F.-X.; Blin, J. A review on pyrolysis of biomass constituents: Mechanisms and composition of the products obtained from the conversion of cellulose, hemicelluloses and lignin. *Renew. Sustain. Energy Rev.* **2014**, *38*, 594–608. [CrossRef]
26. Zhao, S.; Sun, Y.; Lu, X.; Li, Q. Energy consumption and product release characteristics evaluation of oil shale non-isothermal pyrolysis based on TG-DSC. *J. Pet. Sci. Eng.* **2020**, *187*, 106812. [CrossRef]
27. Han, L.; Ro, K.S.; Sun, K.; Jin, J.; Libra, J.A.; Xing, B. New evidence for high sorption capacity of hydrochar for hydrophobic organic pollutants. *Environ. Sci. Technol.* **2016**, *50*, 13274–13282. [CrossRef]
28. Hu, S.; Zhang, D.; Yang, Y.; Ran, Y.; Mao, J.; Chu, W.; Cao, X. Effects of the chemical structure, surface, and micropore properties of activated and oxidized black carbon on the sorption and desorption of phenanthrene. *Environ. Sci. Technol.* **2019**, *53*, 7683–7693. [CrossRef]
29. Zhuo, C.; Hu, S.; Yang, Y.; Ran, Y. Effects of the structures and micropores of sedimentary organic matter on the oxidative degradation of benzo(a)pyrene by Na2S2O8. *Water Res.* **2020**, *174*, 115635. [CrossRef]
30. Hu, S.; Xu, D.; Kong, X.; Gong, J.; Yang, Y.; Ran, Y.; Mao, J. Effect of the structure and micropore of activated and oxidized black carbon on the sorption and desorption of nonylphenol. *Sci. Total Environ.* **2021**, *761*, 144191. [CrossRef]
31. Chu, G.; Zhao, J.; Huang, Y.; Zhou, D.; Liu, Y.; Wu, M.; Peng, H.; Zhao, Q.; Pan, B.; Steinberg, C.E.W. Phosphoric acid pretreatment enhances the specific surface areas of biochars by generation of micropores. *Environ. Pollut.* **2018**, *240*, 1–9. [CrossRef]
32. Ma, H.Z.; Allen, H.E.; Yin, Y.J. Characterization of isolated fractions of dissolved organic matter from natural waters and a wastewater effluent. *Water Res.* **2001**, *35*, 985–996. [CrossRef]
33. Xiao, F.; Pignatello, J.J. Interactions of triazine herbicides with biochar: Steric and electronic effects. *Water Res.* **2015**, *80*, 179–188. [CrossRef] [PubMed]
34. Ji, L.; Wan, Y.; Zheng, S.; Zhu, D. Adsorption of tetracycline and sulfamethoxazole on crop residue-derived ashes: Implication for the relative importance of black carbon to soil sorption. *Environ. Sci. Technol.* **2011**, *45*, 5580–5586. [CrossRef] [PubMed]
35. Xiao, F.; Pignatello, J.J. Effects of post-pyrolysis air oxidation of biomass chars on adsorption of neutral and ionizable compounds. *Environ. Sci. Technol.* **2016**, *50*, 6276–6283. [CrossRef] [PubMed]
36. Feng, D.D.; Guo, D.W.; Zhang, Y.; Sun, S.Z.; Zhao, Y.J.; Shang, Q.; Sun, H.L.; Wu, J.Q.; Tan, H.P. Functionalized construction of biochar with hierarchical pore structures and surface O-/N-containing groups for phenol adsorption. *Chem. Eng. J.* **2021**, *410*, 127707. [CrossRef]
37. Zheng, H.; Wang, Z.Y.; Zhao, J.; Herbert, S.; Xing, B.S. Sorption of antibiotic sulfamethoxazole varies with biochars produced at different temperatures. *Environ. Pollut.* **2013**, *181*, 60–67. [CrossRef]
38. Ling, C.; Li, X.; Zhang, Z.; Liu, F.; Deng, Y.; Zhang, X.; Li, A.; He, L.; Xing, B. High adsorption of sulfamethoxazole by an amine-modified polystyrene-divinylbenzene resin and its mechanistic insight. *Environ. Sci. Technol.* **2016**, *50*, 10015–10023. [CrossRef]
39. Wu, M.; Pan, B.; Zhang, D.; Xiao, D.; Li, H.; Wang, C.; Ning, P. The sorption of organic contaminants on biochars derived from sediments with high organic carbon content. *Chemosphere* **2013**, *90*, 782–788. [CrossRef]